Journal of ELECTRONIC MATERIALS, Vol. 46, No. 6, 2017
DOI: 10.1007/s11664-016-5248-0

Origin of Room Temperature Ferromagnetism in Cr-Doped Lead-Free Ferroelectric $Bi_{0.5}Na_{0.5}TiO_3$ Materials

L.T.H. THANH,[1,2] N.B. DOAN,[3,4,5] N.Q. DUNG,[6] L.V. CUONG,[5] L.H. BAC,[1] N.A. DUC,[7] P.Q. BAO,[2] and D.D. DUNG[1,8]

1.—School of Engineering Physics, Ha Noi University of Science and Technology, 1 Dai Co Viet Road, Hanoi, Viet Nam. 2.—Faculty of Physics, College of Science, Ha Noi National University, 334 Nguyen Trai Road, Hanoi, Viet Nam. 3.—CNRS, Institut Néel, 38042 Grenoble, France. 4.—Univ. Grenoble Alpes, Institut Néel, 38042 Grenoble, France. 5.—Faculty of Engineering Physics and Nanotechnology, University of Engineering and Technology, Vietnam National University, Building E3, 144 Xuan Thuy, Cau Giay, Hanoi, Viet Nam. 6.—Department of Chemistry, Thai Nguyen University of Education, 20 Luong Ngoc Quyen Street, Thai Nguyen, Viet Nam. 7.—Vietnam Maritime University, 48 Lach Tray Street, Ngo Quyen, Haiphong, Viet Nam. 8.—e-mail: dung.dangduc@hust.edu.vn

The development of multiferroic materials based on lead-free ferroelectric material provides an opportunity to fabricate next-generation electronic devices. In this work, Cr-doped lead-free ferroelectric $Bi_{0.5}Na_{0.5}TiO_3$ materials were synthesized by using the sol–gel method. The optical band gap was reduced from 3.12 eV to 2.12 eV for undoped and 9 mol.% Cr-doped $Bi_{0.5}Na_{0.5}TiO_3$ with the substitution of Cr at the Ti-site. Cr-doped $Bi_{0.5}Na_{0.5}TiO_3$ materials exhibited weak ferromagnetism at room temperature. Saturation magnetization was approximately 0.08 μ_B/Cr at 5 K. Our work will facilitate the further understanding of the role of transition metal ferromagnetism in lead-free ferroelectric materials at room temperature.

Key words: $Bi_{0.5}Na_{0.5}TiO_3$, sol-gel, ferromagnetic, lead-free ferroelectric

INTRODUCTION

Research on multiferroic materials rapidly develops because these materials can be used to fabricate a memory device based on the combination of ferromagnetism and ferroelectricity in one material.[1,2] In particular, they provide an opportunity to switch magnetism with an electric field or switch its electric polarity with a magnetic field.[1,2] Recently, multiferroic materials are integrated on a silicon chip to develop electronic devices.[3,4] However, multiferroic materials rarely exist naturally because the conditions to obtain both ferroelectric and ferromagnetic properties are difficult to achieve because of common atomic-level mechanisms.[5,6] Therefore, obtaining multiferroic materials at room temperature remains a major challenge.

Room-temperature ferromagnetism was observed recently in various transition metals, e.g., Fe-, Mn-, and Ni-doped lead-based $PbTiO_3$ ferroelectric materials.[7–9] Room-temperature ferromagnetism in lead-based ferroelectric $PbTiO_3$ also exists with oxygen vacancies.[10] In addition, the composite and/or multilayer ferroelectric/ferromagnetic-based or lead-based ferroelectric $PbTiO_3$, such as $PbTiO_3$–$CoFe_2O_4$ composites,[11] $[PbTiO_3]_{85}/[CoFe_2O_4]_{15}$, and epitaxial thin films,[12] also exhibits room-temperature ferromagnetism. These results present considerable potential to develop the next-generation lead-based piezoelectric and ferroelectric materials. Nevertheless, lead is a hazardous material that pollutes the environment and is harmful to human health. Thus, considerable effort has been devoted toward the development of lead-free multiferroic materials.[13–15]

$Bi_{0.5}Na_{0.5}TiO_3$ and $Bi_{0.5}K_{0.5}TiO_3$ materials and their solid solutions are widely studied as lead-free ferroelectric materials.[16] Hence, the influence of room-temperature ferromagnetism on lead-free ferroelectric materials can possibly fabricate the next-generation electronic devices. Recently, room-temperature ferromagnetism was obtained in

(Received October 2, 2017; accepted December 19, 2016; published online January 6, 2017)

Fe-doped lead-free ferroelectric $Bi_{0.5}K_{0.5}TiO_3$ nanocrystals.[17] Our theory also predicted that the optical band gap reduces in the presence of iron conduction bands, and the ferromagnetism in Fe-doped $Bi_{0.5}K_{0.5}TiO_3$ samples results from the exchange splitting between spin sub-bands based on crystal field theory.[17] Moreover, the possible induction of room-temperature ferromagnetism by Ni-doped lead-free $Bi_{0.5}K_{0.5}TiO_3$ samples could intrinsically be caused by the presence of Ni ions in $Bi_{0.5}K_{0.5}TiO_3$ crystals.[18] Similarly, room-temperature ferromagnetism was reported for transition metal (Co, Fe, and Mn)-doped lead-free ferroelectric $Bi_{0.5}Na_{0.5}TiO_3$materials.[19–21]

In the present work, room-temperature weak-ferromagnetism was obtained in Cr-doped $Bi_{0.5}Na_{0.5}TiO_3$ materials. The reduction of the optical band gap from 3.12 eV to 2.12 eV for undoped and 9 mol.% Cr-doped $Bi_{0.5}Na_{0.5}TiO_3$was caused by the substitution of Cr at the Ti-site. Saturation magnetization was around 0.08 μ_B/Cr at 5 K.

EXPERIMENT

$Bi_{0.5}Na_{0.5}TiO_3$ pure and Cr-doped $Bi_{0.5}Na_{0.5}TiO_3$ (named as BNT pure and BNT-xCr, respectively) samples were synthesized by the sol-gel method. The raw materials consisted of bismuth nitrate pentahydrate ($Bi(NO_3)_2.5H_2O$), sodium nitrate ($NaNO_3$), chromium nitrate ($Cr(NO_3)_3.9H_2O$), and tetraisopropoxytitanium (IV) ($C_{12}H_{28}O_4Ti$). Acetic acid (CH_3COOH) and acetylacetone ($CH_3COCH_2COCH_3$) were selected as solvents. First, bismuth nitrate pentahydrate, sodium nitrate, and chromium nitrate were dissolved in acetic acid and distilled water until they were transparent. Subsequently, acetylacetone was introduced into a prepared solution after adding tetraisopropoxytitanium (IV). The solutions were stirred for around 5 h at room temperature. The sol was heated at 100°C to prepare dry gels. The dry gels were ground and calcined at 400°C for 2 h and sintered at 900°C for 3 h. After sintering, the sample compositions were confirmed by electron probe microanalysis. Thus, sodium was added to an excess of approximately 30 mol.% to prevent sodium loss during the gel and sintering process. Afterward, the white sodium bismuth titanate and yellow chromium-doped sodium titanate powders were obtained. The morphology of these powders was observed by field emission scanning electron microscope (FE-SEM). The crystalline structures of the samples were characterized by x-ray diffraction (XRD). The vibrational and rotational modes were characterized by Raman spectroscopy, and the optical properties were studied by ultraviolet–visible spectroscopy (UV–Vis). Magnetic properties were characterized by using a superconducting quantum interference device (SQUID) magnetometer at 5 K and a vibration sample magnetometer (VSM) at room temperature.

RESULTS AND DISCUSSION

Figure 1 shows the surface morphology of undoped and Cr-doped $Bi_{0.5}Na_{0.5}TiO_3$ samples. The undoped $Bi_{0.5}Na_{0.5}TiO_3$ samples showed inhomogeneous grain size. The grain size of Cr-doped $Bi_{0.5}Na_{0.5}TiO_3$ samples was smaller than that of the un-doped sample. However, the small particles in doped samples tended to aggregate to obtain a large size.

Figure 2a shows the XRD patterns of BNT pure and BNT-xCr samples prepared by the sol-gel method. The observed peak positions and relative intensities were indexed with the standard data of the $Bi_{0.5}Na_{0.5}TiO_3$ compound and confirmed the rhombohedral perovskite structure of all prepared samples. These results were in agreement with the patterns reported in the literature.[22,23] All samples showed a single phase with perovskite structure. The impurity phase was not observed, even in a logarithmically scaled θ–2θ XRD pattern. Comparison of the location of (003) diffraction peaks in the range of 44°–49° showed that the peak positions of Cr-doped samples slightly shifted toward higher 2θ values, as shown in Fig. 2b. The distorted structure indicated that Cr incorporated with the lattice structure and compressed the lattice parameters. Nevertheless, such a result is unexpected because of the same ionic radii of Cr^{3+}(0.0615 nm) and Ti^{4+} (0.061 nm) in six coordination.[24] Cr^{3+}substituted at the Ti^{4+}site, thereby the oxygen defects in the lattice were because of the unbalanced charge state. Becerro et al. reported that vacancy ordering starts from isolated oxygen vacancies randomly distributed in the lattice.[25] Jedvik et al. reported that the size of the oxygen vacancy ion is smaller than that of an oxygen ion.[26] Shanh et al. suggested that oxygen defects caused by Cr^{3+} doping could distort the $BaTiO_3$ structure.[27] Therefore, we suggested that oxygen vacancies resulted in a compressed lattice structure because of the dominance effect from the compression of radii Cr^{3+}ion dopant and Ti^{4+}ion host.

Figure 3a shows the Raman spectra of BNT pure and BNT-xCr at room temperature in the wave number range of 100–700 cm^{-1}. The Raman bands for BNT pure and BNT-xCr were relatively broad, which resulted from the disorder on the A-site and from overlapping Raman modes. Thus, the different modes were difficult to distinguish. For a close inspection and reliable comparison, the spectral properties of samples were fitted to an equal number of Lorentzian peaks, as shown in Fig. 3b and c for BNT pure and 5 mol.% and BNT-xCr, respectively. These results indicated that the intensity of local peaks at around 490 cm^{-1} increased with increasing Cr dopant concentration. Niranjan et al. predicted that the lowest frequency modes in the range of 109–134 cm^{-1} are dominated by the displacement of Bi ions, and the modes in the frequency range of 155–187 cm^{-1} and 246–401 cm^{-1} are dominated by Na-O and TiO_6

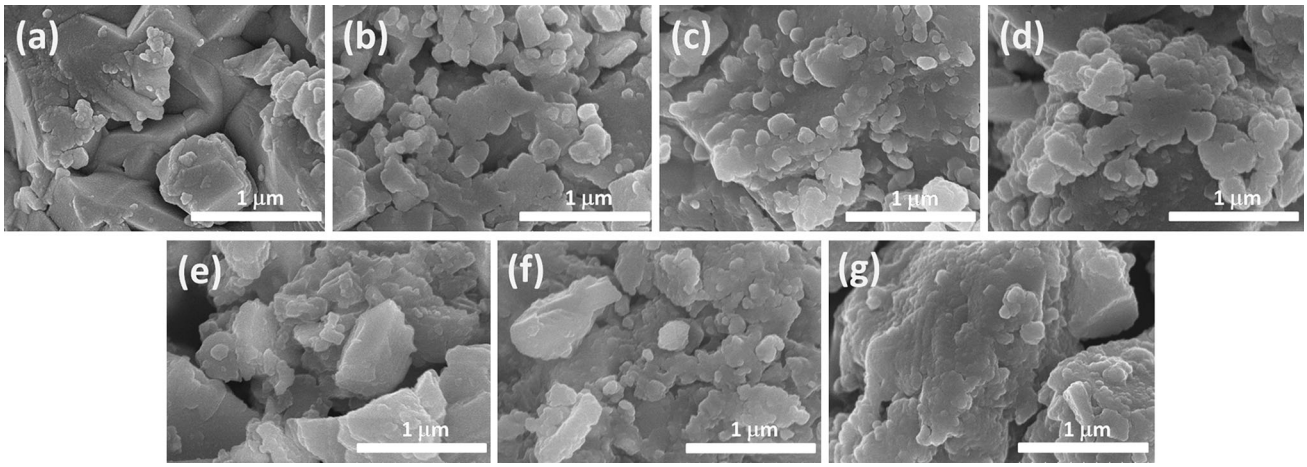

Fig. 1. Surface homology of (a) undoped $Bi_{0.5}Na_{0.5}TiO_3$ and (b)–(g) Cr-doped $Bi_{0.5}Na_{0.5}TiO_3$ samples with 0.5 mol.%, 1 mol.%, 3 mol.%, 5 mol.%, 7 mol.%, and 9 mol.%, respectively.

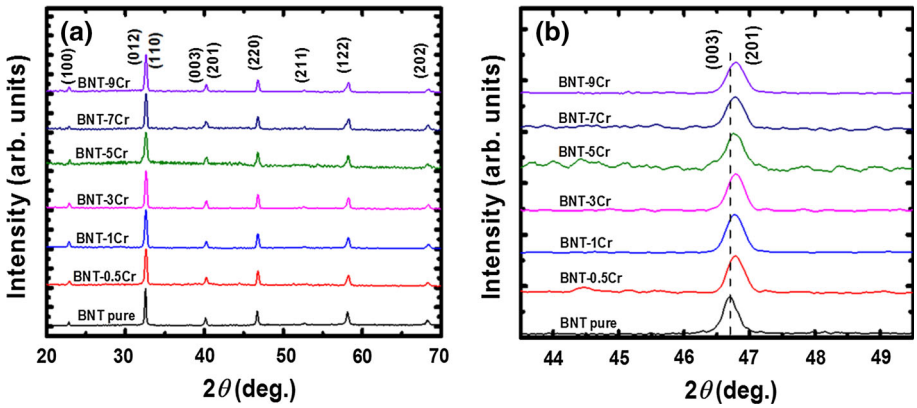

Fig. 2. (a) X-Ray diffraction pattern of $Bi_{0.5}Na_{0.5}TiO_3$samples as a function of Cr doping concentration and (b) a comparison of (003) diffraction peak positions.

vibrations, respectively. The high frequency modes in the range 413–826 cm^{-1} are primarily associated with oxygen atom vibrations.[28] The vibration at around 490 $cm^{-1}$is the longitudinal A_1(LO7) optical modes.[28] In addition, the appearance of a blue-shifted shoulder at 260 cm^{-1} and 303 cm^{-1} peaks is related to the increased distortion of TiO_6(CrO_6) octahedral configuration with increasing Cr concentration. Our results were consistent with recent reports for $Bi_{0.5}Na_{0.5}TiO_3$ solid solution with $BiCrO_3$.[29]

Figure 4a shows the optical absorption spectra of $Bi_{0.5}Na_{0.5}TiO_3$samples doped with various Cr concentrations. The absorption edge showed an obvious red shift for the BNT-xCr samples, thereby indicating that the band gap (E_g) was reduced. These results were further evident for Cr^{3+} cation incorporation into the crystal structure of $Bi_{0.5}Na_{0.5}TiO_3$. Furthermore, the absorbance peak at around 436 nm suggested the Cr^{3+} local states. E_g values were calculated by using the plot of $(\alpha h\nu)^2$ versus photon energy $h\nu$,as shown in Fig. 4b, where α is the absorbance coefficient, h is the Planck constant, and ν is the frequency. The optical band gap was 3.11 eV for BNT pure and 2.12 eV for and 9 mol.% BNT-xCr. Inset in Fig. 4b shows the band gap values as a function of Cr doping concentration. These results were consistent with our recent work that the band gap of lead-free ferroelectric $Bi_{0.5}K_{0.5}TiO_3$materials is altered via Fe- and Ni-substitutions at the Ti-site.[17,18] Thus, we suggested that incorporation of d orbital electronics into the lattice by Cr ion doping reduced the band gap of $Bi_{0.5}Na_{0.5}TiO_3$ materials.

Furthermore, the effect of d electrons on the ferromagnetic properties of $Bi_{0.5}Na_{0.5}TiO_3$ materials was observed by determining the magnetic moment versus the magnetic field plot of BNT pure and BNT-xCr samples (Fig. 5). Figure 5a shows the magnetic hysteresis (M–H) loops of the BNT pure and BNT-xCr samples at room temperature. The hysteresis loop showed an anti-S shape. This shape could be attributed to the competition between ferromagnetic and diamagnetic contributions to the magnetism of the samples. The diamagnetic

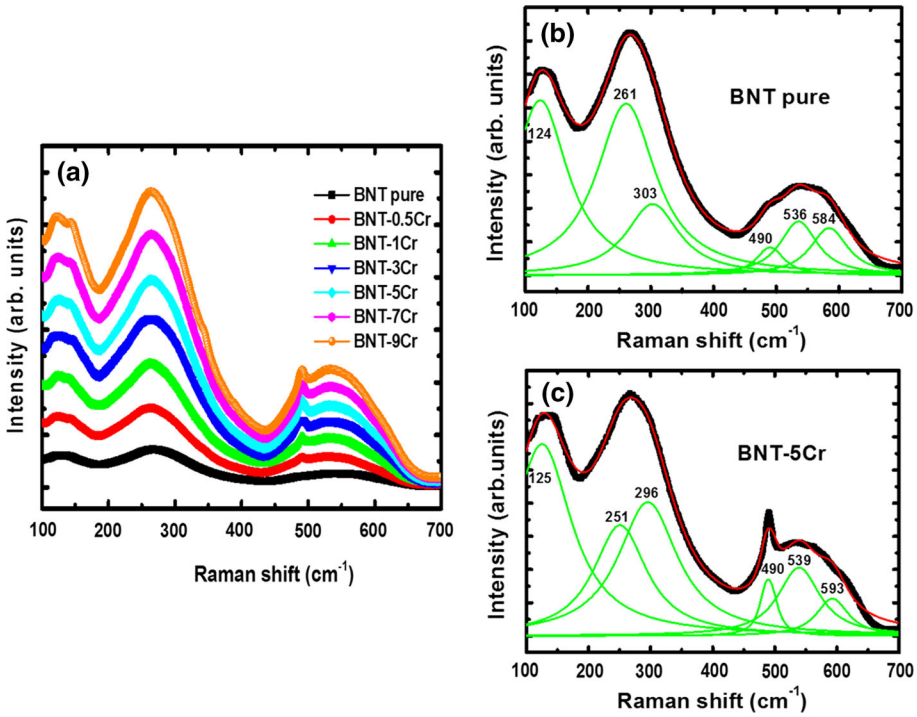

Fig. 3. (a) Raman spectra of the $Bi_{0.5}Na_{0.5}TiO_3$ samples as a function of Cr doping concentration. (b) and (c) Spectra deconvolution of pure and Cr-doped $Bi_{0.5}Na_{0.5}TiO_3$with 5 mol.% samples, respectively.

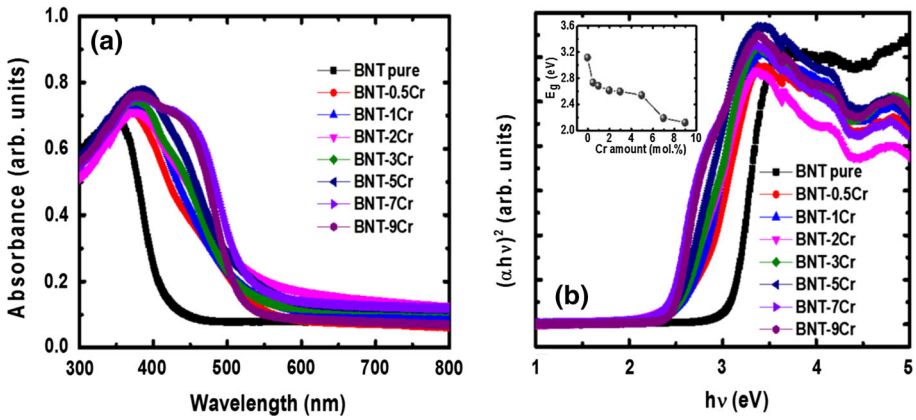

Fig. 4. (a) UV–Vis absorption spectra and (b) the dependence of $(\alpha h\nu)^2$ on the photon energy ($h\nu$) of pure and Cr-doped $Bi_{0.5}Na_{0.5}TiO_3$ samples. The inset in (b) shows the band gap E_g of $Bi_{0.5}Na_{0.5}TiO_3$ samples as a function of Cr dopant.

nature of $Bi_{0.5}Na_{0.5}TiO_3$ provides evidence that Ti ions are in the 4 + state with d^0 electrons, a behavior similar to that of $BaTiO_3$.[27] In vacancy-induced magnetism of ferroelectric $Bi_{0.5}Na_{0.5}TiO_3$ materials, the magnetism of materials with neutral Na or Ti vacancies mainly originated from the polarization of O 2*p* electrons.[30] We also reported the room-temperature ferromagnetism of various oxides with perovskite structure, such as $PbTiO_3$, $BaTiO_3$, or $SrTiO_3$, which resulted from defect O- and/or Ti vacancy.[8,10,31,32] The observed weak ferromagnetism of $Bi_{0.5}Na_{0.5}TiO_3$ at room temperature was suggested by the presentation of self-defect vacancies, such as in Ti and O. Diamagnetism of $Bi_{0.5}Na_{0.5}TiO_3$ is transformed to ferromagnetism by Fe-, Co-, and Mn-doping.[19–21] The weak diamagnetic signal was converted to a weak ferromagnetic loop with the incorporation of Cr in the $Bi_{0.5}Na_{0.5}TiO_3$ lattice. This result confirmed the ferromagnetism in a low magnetic field. Unlike Fe-, Co- or Mn-doped $Bi_{0.5}Na_{0.5}TiO_3$, diamagnetism could not change to a clear S-shape, which indicated the significant Cr-induced weak-ferromagnetism via substitution at the Ti-site than that of Fe-, Co- or Mn- dopants. The clear evidence for a ferromagnetism hysteresis loop is shown in the Fig. 5a inset

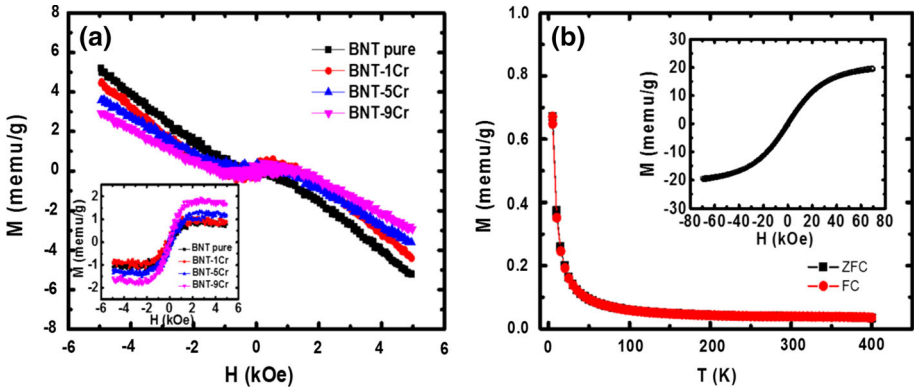

Fig. 5. (a) Magnetic hysteresis (*M–H*) curves of the Cr-doped $Bi_{0.5}Na_{0.5}TiO_3$ samples. The inset shows the *M–H* curve of the un-doped and Cr-doped $Bi_{0.5}Na_{0.5}TiO_3$ after subtraction of the diamagnetic component. (b) *M–T* curve at 1 kOe magnetic field for 1 mol.% Cr-doped $Bi_{0.5}Na_{0.5}TiO_3$ samples under zero field cooling (ZFC) and field cooling (FC) modes. The inset shows the *M–H* curve of a 1 mol.% Cr-doped $Bi_{0.5}Na_{0.5}TiO_3$ sample at 5 K.

after subtracting the diamagnetic component. In addition, the un-doped $Bi_{0.5}Na_{0.5}TiO_3$ samples also exhibited weak ferromagnetism at room temperature. The coercive field (H_C) and remanence magnetization (M_r) were around 150 Oe and 0.3 memu/g, respectively. These parameters were solid evidence for ferromagnetism behavior at room temperature. The H_C value of Cr-doped $Bi_{0.5}Na_{0.5}TiO_3$ samples was consistent with previously reported values for transition metal-doped ferroelectric materials, such as $H_C \sim 100$ Oe for Fe-doped $Na_{0.5}Bi_{0.5}TiO_3$ and $PbTiO_3$ or $H_C \sim 135$ Oe for Mn-doped $PbTiO_3$.[7–9,20] These results were also consistent with our previously reported values for Fe- and Ni-doped $Bi_{0.5}K_{0.5}TiO_3$ with H_C of around 70 Oe and 120 Oe, respectively.[17,18]

Figure 5b shows the dependence of magnetization on temperature below zero field cooling (ZFC) and field cooling (FC) modes. The measurement was carried out under an applied field of 1 kOe of $Bi_{0.5}Na_{0.5}Ti_{0.99}Cr_{0.01}O_3$ samples. The inset in Fig. 4b shows the *M–H* curve of $Bi_{0.5}Na_{0.5}Ti_{0.99}Cr_{0.01}O_3$ samples under 70 kOe at 5 K. The maxima magnetization (M_S) was $\sim$ 19.8memu/g at 5 K, which corresponds to 0.08 μ_B/Cr. Shah et al. reported that incorporation of Cr^{3+} ions at the Ti^{4+} ion sites in $BaTiO_3$ will create oxygen vacancies and induce O(p)–Cr(d) hybridization. Thus, the charge carriers involved in bonding mediate the exchange interaction via oxygen vacancies among the local spins, thereby resulting in ferromagnetism.[26] Inaba et al. found weak ferromagnetic behavior through substitution of Cr for Ti in $SrTiO_3$, which results from carrier-mediated exchange interactions between the Cr ions.[33] The exchange interactions between localized electron spin moments and oxygen vacancies on the surface of nanoparticles were originally observed at room temperature.[34] Recently, the first-principle study of magnetism in transition metal-doped $Bi_{0.5}Na_{0.5}TiO_3$ materials indicated that a transition metal atom substitution for a Ti atom produces magnetic moments, which are caused by the spin polarization of transition metal 3*d* electrons.[35] The room temperature ferromagnetism in Fe-doped $Bi_{0.5}K_{0.5}TiO_3$ nanocrystals was explained by first-principle density function theory, which results from the exchange splitting between spin sub-bands through crystal field theory.[17] Therefore, we suggest that the presence of weak-ferromagnetism in Cr-doped $Bi_{0.5}Na_{0.5}TiO_3$ at room temperature was possible with the exchange splitting of transition metals at the octahedral site and/or enhancement via oxygen vacancies.

CONCLUSION

Weak-ferromagnetism at room temperature was obtained in un-doped and Cr-doped lead-free ferroelectric $Bi_{0.5}Na_{0.5}TiO_3$ materials. The optical band gap was reduced from 3.12 eV to 2.12 eV for BNT pure and 9 mol.% BNT-xCr, which resulted from the substitution of Cr at the Ti-site. This work can further the understanding of the role of transition metals in ferroelectric materials to develop environmentally friendly multiferroic materials based on lead-free ferroelectric materials.

ACKNOWLEDGEMENT

This research was funded by the Vietnam National Foundation for Science and Technology Development (NAFOSTED) under Grant Number 103.02-2015.89.

REFERENCES

1. T. Kimura, T. Goto, H. Shintani, K. Ishizaka, T. Arima, and Y. Tokura, *Nature* 426, 55 (2003).
2. N. Hur, S. Park, P.A. Sharma, J.S. Ahn, S. Guha, and S.W. Cheong, *Nature* 429, 392 (2004).
3. S.R. Singamaneni, W. Fan, J.T. Prater, and J. Narayan, *J. Appl. Phys.* 116, 224104 (2014).
4. S.R. Singamaneni, S. Punugupati, J.T. Prater, F. Hunte, and J. Narayan, *J. Appl. Phys.* 116, 094103 (2014).
5. N.A. Spaldin and M. Fiebig, *Science* 309, 391 (2005).
6. N.A. Hill, *J. Phys. Chem. B* 104, 6694 (2000).
7. Z. Ren, G. Xu, X. Wei, Y. Liu, X. Hou, P. Du, W. Weng, G. Shen, and G. Han, *Appl. Phys. Lett.* 91, 063106 (2007).

8. L.M. Oanh, D.B. Do, N.D. Phu, N.T.P. Mai, and N.V. Minh, *IEEE Trans. Magn.* 50, 2502004 (2014).
9. L.M. Oanh, D.B. Do, and N.V. Minh, *Mater. Trans.* 56, 1358 (2015).
10. T. Shimada, Y. Uratani, and T. Kitamura, *Appl. Phys. Lett.* 100, 162901 (2012).
11. B.Y. Wang, H.T. Wang, S.B. Singh, Y.C. Shao, Y.F. Wang, C.H. Chuang, P.H. Yeh, J.W. Chiou, C.W. Pao, H.M. Tsai, H.J. Lin, J.F. Lee, C.Y. Tsai, W.F. Hsieh, M.H. Tsai, and W.F. Pong, *RSC Adv.* 3, 7884 (2013).
12. M. Murakami, K.S. Chang, M.A. Aronova, C.L. Lin, M.H. Yu, J.H. Simpers, M. Wuttig, and I. Takeuchi, *Appl. Phys. Lett.* 87, 112901 (2005).
13. W. Jo, R. Dittmer, M. Acosta, J. Zang, C. Groh, E. Sapper, K. Wang, and J. Rodel, *J. Electroceram.* 29, 71 (2012).
14. Y. Li, K.S. Moon, and C.O. Wong, *Science* 380, 1419 (2005).
15. E. Cross, *Nature* 432, 24 (2004).
16. N.D. Quan, L.H. Bac, D.V. Thiet, V.N. Hung, and D.D. Dung, *Adv. Mater. Sci. Eng.* 2014, 365391 (2014).
17. D.D. Dung, D.V. Thiet, D. Odkhuu, L.V. Cuong, N.H. Tuan, and S. Cho, *Mater. Lett.* 156, 129 (2015).
18. D.V. Thiet, D.D. Cuong, L.H. Bac, L.V. Cuong, H.D. Khoa, S. Cho, N.H. Tuan, and D.D. Dung, *Mater. Trans.* 56, 1339 (2015).
19. Y. Wang, G. Xu, X. Ji, Z. Ren, W. Weng, and P. Du, *J. Alloys Compd.* 475, L25 (2009).
20. Y. Wang, G. Xu, L. Yang, Z. Ren, X. Wei, and W. Weng, *Mater. Sci.* 27, 471 (2009).
21. L.T.H. Thanh, N.B. Doan, L.H. Bac, D.V. Thiet, S. Cho, P.Q. Bao, and D.D. Dung, *Mater. Lett.* 186, 239 (2017).
22. H. Nagata and T. Takenaka, *J. Eur. Ceram. Soc.* 21, 1299 (2001).
23. A. Watcharapason, S. Jiansirisomboon, and T. Tunkasiri, *Mater. Lett.* 61, 2986 (2007).
24. R.D. Shannon, *Acta. Cryst. A* 32, 751 (1976).
25. A.I. Becrreo, C. McCammon, F. Langenhorst, F. Seifert, and R. Angel, *Phase Trans.* 69, 133 (1999).
26. E. Jedvik, A. Lindman, M.P. Benediktsson, and G. Wahnstrom, *Solid State Ionics* 275, 2 (2015).
27. J. Shah and R.K. Kotnala, *J. Mater. Chem. A* 1, 8601 (2013).
28. M.K. Niranjan, T. Karthik, S. Asthana, J. Pan, and U.V. Waghmare, *J. Appl. Phys.* 113, 194106 (2013).
29. R. Selvamani, G. Singh, V. Sathe, V.S. Tiwari, and P.K. Gupta, *J. Phys.: Condens. Mater.* 23, 055901 (2011).
30. Y. Zhang, J. Hu, F. Gao, H. Liu, and H. Qin, Comput. *Theor. Chem.* 967, 284 (2011).
31. T.L. Phan, P. Zhang, D.S. Yang, T.D. Thanh, D.A. Tuan, and S.C. Yu, *J. Appl. Phys.* 113, 17E305 (2013).
32. I.R. Shein and A.L. Ivanovskii, *Phys. Lett. A* 317, 155 (2007).
33. J. Inaba and T. Katsufuji, *Phys. Rev. B* 72, 052408 (2005).
34. A. Sundaresan, R. Bhargavi, N. Rangarajan, U. Siddesh, and C.N.R. Rao, *Phys. Rev. B* 74, 161306 (2006).
35. L. Ju, T.S. Xu, Y.J. Zhang, and L. Sun, *Chin. J. Chem. Phys.* 29, 426 (2016).